ISSN 1392-1207. MECHANIKA. Vol. 30, No. 1, 2024: 74–82

An Adaptive Extended Finite Element Based Crack Propagation Analysis Method

Guizhong XIE*, Chongmao ZHAO*, Hao LI*, Jun LIU, Yudong ZHONG*, Wenliao DU*, Jiahe LV***, Chao WU***

**Henan Provincial Key Laboratory of Intelligent Manufacturing of Mechanical, Mechanical and Electrical Engineering Institute, Zhengzhou University of Light Industry, Zhengzhou, 450002, Henan, China, E-mails: xieguizhong@126.com; 2250717725@qq.com; lihao@zzuli.edu.cn; zhongyd@zzuli.edu.cn; dwenliao@zzuli.edu.cn; wuchao7379@163.com*
***State Key Laboratory of Mining Heavy equipment, CITIC Heavy Industries CO., LTD, Luoyang 471039, China, E-mail: ustblj@163.com*
****Faculty of Engineering, China University of Geosciences, Wuhan 430074, China, E-mail: lvjiahe@cug.edu.cn*
https://doi.org/10.5755/j02.mech.33301

1. Introduction

In engineering structures, the existence of cracks will reduce strength and life, causing serious safety accidents and economic losses. In recent years, with the rapid development of computational science, computational mechanics is widely used in crack analysis, including finite element method (FEM) [1-3], meshless methods (MMs) [4-6], boundary element method (BEM) [7-10], XFEM [11-13], etc. However, the traditional finite element method relies too much on the mesh, which leads to the complexity of the pre-processing of crack growth. As the crack grows, the mesh of each propagation needs to be re-divided, which increases the additional calculation cost. In addition, because the conventional finite element can not reflect the nature of the crack tip, a large number of the mesh needs to be divided to obtain displacement and stress fields with higher accuracy. MMs can completely or partially eliminate the mesh, without mesh division and reconstruction [14-15]. However, MMs are difficult to deal with the convergence of discrete functions and require a large amount of computation [16], with low computational efficiency, whose convergence, consistency, and error analysis lack a solid theoretical basis and mathematical proof. The BEM will encounter problems of singular integral and nearly singular integrals [17-19]. When encountering nonlinear terms, it needs to deal with the corresponding area integral. The XFEM is based on the extended shape functions to capture the discontinuities in the region, including cracks, holes, inclusions, material interfaces, etc. [20-21]. The description of the discontinuity is completely independent of the computational mesh, and the discontinuity at the crack tip is captured by introducing a strengthening function. The level set method is used to characterize the crack, which has a great advantage in dealing with the crack problem. For the introduction of the level set method, Bordas [22] et al. combined the XFEM with the level set method to solve the fracture problem of complex three-dimensional engineering structures. At the same time, the capture of crack characteristics does not rely on the extended finite element mesh. When simulating crack growth, it avoids remeshing and improves the calculation efficiency while maintaining the calculation accuracy. Moës, Nicolas and Belytschko [23] et al. further improved the XFEM, using step function and crack tip functions to strengthen the element. Budyn, Zi, Moës [24] et al. studied the multi crack problem of brittle materials using the XFEM. Wells [25], Belytschko [26], Asferg, Poulsen, and other scholars [27] applied the cohesive crack model to the elastoplastic fracture problem of extended finite elements. However, for the actual complex fracture structure, the calculation accuracy of XFEM is difficult to meet [28], and the simulation results have little referential importance for these problems. It is well known that the importance of practical application depends on the stress intensity factor [29]. Therefore, the mesh adaptive technology is introduced to refine the mesh near the crack tip area through error analysis, which can effectively improve the calculation accuracy.

The mesh adaptive technology [30-32] is based on error estimation to reconstruct the mesh in areas with excessive errors to obtain more accurate solutions until they meet the calculation requirements. The advantage of the adaptive method is that it can evaluate the quality of the current mesh, densify the local mesh, and control the increase of structural degrees of freedom to improve the calculation accuracy [34]. Yulong Shao [33] et al. proposed a thinning criterion about the history of the maximum residual strain energy. Based on the background mesh insertion node, it is proved that the results combined with the adaptive method are more accurate. De Oliveira Miranda [35] et al. studied the mesh refinement problem and related errors when using the FEM to calculate the SIFs. In the XFEM framework, Wang [36] realized the mesh refinement of the interface among the features such as inclusions, holes through variable node element method. Tabarraei [37] used polygonal mesh and quadtree mesh to calculate the crack growth problem by constructing the approximate space of polygonal elements. In this paper, we make mesh adaptive technology improvements to the XFEM solution process, judge whether the current results can meet the calculation requirements through error analysis, and reconstruct the mesh in the area with low calculation accuracy according to the analysis results. Firstly, according to the geometric characteristics of the structural model, the boundary conditions are divided into initial mesh for XFEM calculation. Analyze the error of the calculation results to determine whether the accuracy meets the set requirements. If the accuracy is not enough, refine the mesh and continue the calculation. If the accuracy meets the requirements, continue the next step of the calculation. Thus, the calculation accuracy can be improved without increasing too much calculation burden. The combination of adaptive technology and XFEM can calculate the SIFs accurately at the crack tip and predict the crack propagation.

Our goal is to improve the computational accuracy of XFEM for crack propagation problems. The accuracy of the calculation results is improved without increasing the calculation cost, and the practical significance is better satisfied by local encryption of the broken mesh.

The structure of this paper is as follows. In Section 2, numerical derivations of the level set function and XFEM are described in detail. In section 3, the calculation method of SIFs and the mathematical formula of crack propagation prediction by SIFs are given. In section 4, the formula of grid adaptive technique is introduced. In Section 5, the static SIF results of two cracked plates are compared to verify the calculation accuracy of the proposed method. The reliability of the proposed method for crack propagation prediction is verified by comparing the results with those without the adaptive method. The conclusion is given in section 6.

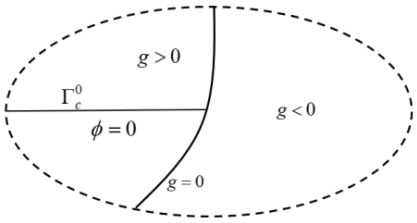

Fig. 1. The crack is represented by the level set function

2. Extended finite element method

In general, the stress at the crack tip is increasing sharply, thus it is necessary to introduce the strengthening function to simulate the strong discontinuity of the crack

$$H(\phi(x)) = \begin{cases} 1 & \phi(x) > 0 \\ -1 & \phi(x) \le 0 \end{cases}, \tag{1}$$

where $\phi(x)$ is the level set function of the crack plane.

The horizontal set method is a numerical method that can determine the position of the interface and track the movement of the interface. The location of the crack surface Γ_c^0. is described in Fig. 1.

During the calculation, the discontinuity always meets

$$\phi\left(x(t),t\right) = 0 . \tag{2}$$

All points meet this condition from a set $\gamma(t)$.

Generally, the signed distance function is used to construct the level set function of the crack surface.

$$\phi(x,t) = \pm \min_{x_\gamma \in \gamma(t)} \left\| x - x_\gamma \right\| . \tag{3}$$

For A discontinuity point with an end point, the crack surface terminates inside the solution domain. Assuming that the moving velocity v_i of the crack end point x_i is known, the level set function corresponding to this end point is defined as:

$$g_i = (x - x_i) \bullet \frac{v_i}{\left\| v_i \right\|} . \tag{4}$$

The crack tip strengthening function $F_l(x)$ of the element near the crack tip is usually a linear combination of Eq. (5).

$$\left\{ F_l(r,\theta) \right\}_{l=1}^{4} = \left[\sqrt{r}\sin\frac{\theta}{2}, \sqrt{r}\cos\frac{\theta}{2}, \sqrt{r}\sin\frac{\theta}{2}\sin\theta, \sqrt{r}\cos\frac{\theta}{2}\sin\theta \right], \tag{5}$$

where r and θ are the parameters defined in polar coordinates around the crack tip.

The approximate displacement expression of the two-dimensional compound crack problem can be obtained as Eq. (6)

$$u(x) = \sum_{j \in J} N_j(x) H(x) \bar{a}_j + \sum_{i \in I} N_i(x) \bar{u}_i + \sum_{k \in K} \left[N_k(x) \sum_{\alpha=1}^{4} F_l(x) \bar{b}_k^l \right], \tag{6}$$

where the unit decomposition functions $N_i(x)$, $N_j(x)$, $N_k(x)$ are the standard finite element form functions. $\bar{u}_i$ is node displacement. $\bar{a}_j$ is the additional degree of freedom of the element which is penetrated by the crack, and $\bar{b}_k^l$ is the additional degree of freedom of the element near the crack tip. They have no clear physical meanings. I is the node set of the solution domain. J is the set of reinforcing nodes through the element. K is the set of reinforcing nodes of the element near the crack tip.

As the approximate expression of displacement is constructed, the discrete numerical equation is deduced according to the principle of virtual work. The governing equation is established considering the equilibrium state of the cracked body under the boundary conditions and loads

$$\begin{cases} \dfrac{\partial \sigma_x}{\partial x} + \dfrac{\partial \tau_{xy}}{\partial y} + f_x = 0 \\ \dfrac{\partial \tau_{xy}}{\partial x} + \dfrac{\partial \sigma_y}{\partial y} + f_y = 0 \end{cases} . \tag{7}$$

The elastic boundary conditions are as follows

$$\sigma \cdot n_t = t \text{ , on } \Gamma_t , \tag{8}$$

$$u = \tilde{u} \text{ , on } \Gamma_u , \tag{9}$$

$$\sigma \cdot n_f = 0 \text{ , on } \Gamma_f . \tag{10}$$

The above equations are expressed in tensor form as: $\nabla\sigma + f^b = 0$, where ∇ represents the differential operator, σ is the stress tensor, f^b is the volume force, t is the

boundary stress vector, $\tilde{u}$ is the boundary displacement vector, n is the inter-face normal vector.

The finite element integral equation is obtained by introducing the arbitrary displacement $\phi^T = (\phi_x, \phi_y)$ at the equilibrium position

$$\int_A \left[\begin{array}{l} \left(\dfrac{\partial \sigma_x}{\partial x} + \dfrac{\partial \tau_{xy}}{\partial y} + f \right)_x \phi_x + \\ + \left(\dfrac{\partial \tau_{xy}}{\partial x} + \dfrac{\partial \sigma_y}{\partial y} + f_y \right) \phi_y \end{array} \right] t dA = 0 . \tag{11}$$

The weak form of the integral equation is obtained according to the principle of virtual work

$$\begin{array}{l} -\int_\Omega \sigma^T \varepsilon(\phi) t dA + \int_\Omega \phi^T f t dA + \\ + \int_L \left[\left(n_x \sigma_x + n_y \tau_{xy} \right) \phi_x + \left(n_x \tau_{xy} + n_y \sigma_y \right) \phi_y \right] d\Gamma = 0. \end{array} \tag{12}$$

The discrete numerical equation of the extended finite element is as follows

$$U^h K = F , \tag{13}$$

where U is the total node displacement, $U^h = \{u, a, b_1, b_2, b_3, b_4\}^T$. F is the overall load vector, and F is formed by the load vector f^e of each element. K is the global stiffness matrix, which is formed by the stiffness matrix K^e of each element based on the number group of degrees of freedom in the total stiffness.

The expressions of K^e and f^e are as follows

$$K_{ij}^e = \begin{bmatrix} k_{ij}^{uu} & k_{ij}^{ua} & k_{ij}^{ub} \\ k_{ij}^{au} & k_{ij}^{aa} & k_{ij}^{ab} \\ k_{ij}^{bu} & k_{ij}^{ba} & k_{ij}^{bb} \end{bmatrix}, \tag{14}$$

$$f_i^e = \left\{ f_i^u, f_i^a, f_i^{b1}, f_i^{b2}, f_i^{b3}, f_i^{b4} \right\}^T , \tag{15}$$

where i and j are element node numbers for a four-node linear element, $i, j = 1, 2, 3, 4$.

The extended finite element theory has been very mature, this paper will not do derivation, specific reference can be made to other scholars' literature.

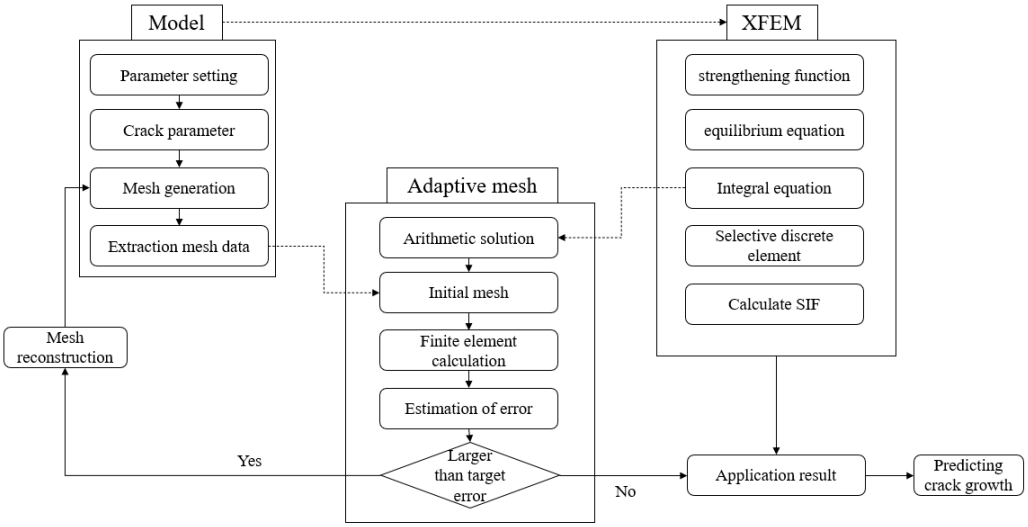

Fig.2. Flow chart of adaptive extension finite element

3. Stress intensity factors calculation and crack propagation prediction

Interaction integral is a high precision SIF calculation method based on the *J* integral method. The expression of *J* integral is

$$J = \int_\Omega \left(W dx_2 - \lambda \frac{\partial u}{\partial x_1} d\eta \right), \tag{16}$$

where η is the integral path, $\lambda = (\lambda_1, \lambda_2)$ is the force per unit length of the integral path, its component $\lambda_i = \sigma_{ij} n_j$, $n = (n_1, n_2)$ is the unit normal vector along the integration path, and $u = (u_1, u_2)$ is the displacement vector.

The strain energy density *W* is

$$W = \frac{1}{2} \sigma_{ij} \varepsilon_{ij} \left(i, j = 1,2 \right), \tag{17}$$

where σ_{ij}, ε_{ij} are the stress and strain components on the integral path.

By introducing the function δ_{1j}, we can obtain

$$\delta_{1j} = \begin{cases} 1 & j = 1 \\ 0 & j = 2 \end{cases}. \tag{18}$$

Substitute Eqs. (17) and (18) into (16) and introduce Green's formula

$$J = \int_\Omega \left(\sigma_{ij} \frac{\partial (u_i)}{\partial x_1} - W \delta_{1j} \right) \frac{\partial q}{\partial x_j} d\eta , \tag{19}$$

where q is any smoothing function, which is 1 in the inner path and 0 in the outer path.

For the composite crack J integral is no longer applicable, we use the interaction integral to calculate the stress intensity factor. The stress and strain of the auxiliary state are selected to satisfy the equilibrium equation and the surface force boundary conditions of the regional crack surface.

$$J = \int_{\Omega}\left(\left(\sigma_{ij}^{real}+\sigma_{ij}^{aux}\right)\frac{\left(\partial u_i^{real}+u_i^{aux}\right)}{\partial x_1}\right)\frac{\partial q}{\partial x_j}d\eta - \\ -\int_{\Omega}\left(\frac{1}{2}\left(\sigma_{ij}^{real}+\sigma_{ij}^{aux}\right)\left(\varepsilon_{ij}^{real}+\varepsilon_{ij}^{aux}\right)\right)\frac{\partial q}{\partial x_j}d\eta, \tag{20}$$

where σ_{ij}^{real}, ε_{ij}^{real}, u_i^{real} are variables of the real stress-strain field, and σ_{ij}^{aux}, ε_{ij}^{aux}, u_i^{aux} are variables of the auxiliary stress-strain field. Define it as the sum of the two states

$$J = J^{real} + J^{aux} + M, \tag{21}$$

where M is the integral of the interaction between two states

$$M = \int_{\Omega}\left(\sigma_{ij}^{real}\frac{\partial u_i^{aux}}{\partial x_1}+\sigma_{ij}^{aux}\frac{\partial u_i^{real}}{\partial x_1}-W^{(real,aux)}\delta_{1j}\right)\frac{\partial q}{\partial x_j}d\eta, \tag{22}$$

when the path Ω approaches the crack tip, the interaction integral has the following relationship with the stress intensity factors of the real deformation field and the additional deformation field

$$M = \frac{2}{E^*}\left(K_I^{real}K_I^{aux}+K_{II}^{real}K_{II}^{aux}\right), \tag{23}$$

where E^* is the combination term of material constant E (Young's modulus) and ν (Poisson's ratio)

$$E^* = \begin{cases} E & \text{Plane strain} \\ \dfrac{E}{1-\nu^2} & \text{Plane stress} \end{cases}. \tag{24}$$

If the auxiliary fields meet the requirements of $K_I^{aux}=1$, $K_{II}^{aux}=0$, the real stress-strain field type I stress intensity factor K_I^{real} can be obtained directly through mutual rental integral. Similarly, if $K_I^{aux}=0$, $K_{II}^{aux}=1$ are satisfied, the type II stress intensity factor K_{II}^{real} of the real stress-strain field can be obtained

$$K = \frac{E'}{2}M\begin{cases}\text{for mod } I.....K_I^{aux}=1\ K_{II}^{aux}=0 \\ \text{for mod } II.....K_I^{real}=0\ K_{II}^{real}=1\end{cases}. \tag{25}$$

In the local coordinate system of the crack tip, the formula of crack growth Angle Θ_c is obtained by setting the shear stress as zero

$$K_I\sin\left(\theta_c\right)+K_{II}\left(3\cos\left(\theta_c\right)-1\right)=0. \tag{26}$$

This is given by the above formula

$$\theta_c = 2\arctan\left(\frac{K_I \pm \sqrt{K_I^2+8K_{II}^2}}{4K_{II}}\right). \tag{27}$$

To prevent the crack from extending in the opposite direction, $|\theta_c|$ must be ensured to be less than $\pi/2$, then the above equation is only taken as a negative sign

$$\theta_c = 2\arctan\left(\frac{K_I - \sqrt{K_I^2+8K_{II}^2}}{4K_{II}}\right), \tag{28}$$

where the positive or negative of θ_c depends on the positive or negative of K_{II}. K_{II} is positive and θ_c is negative, if K_{II} is negative, θ_c is positive. According to the obtained angle, the next propagation direction of the crack can be obtained, and the crack is set as a fixed propagation step. The crack tip position after the first propagation can be obtained, and the calculation is repeated until the crack propagation stops or the structure is destroyed.

4. Adaptive mesh refinement

Adaptive mesh refinement is an optimization method for domain mesh [38]. Using stress smoothing, using smooth stress instead of the exact solution, the improved result is obtained by the following equation

$$\sigma^* = N\bar{\sigma}_i, \tag{29}$$

where $\bar{\sigma}_i$ is the stress of each node calculated by the local smoothing method and the average method.

$$\bar{\sigma}_i = \frac{\sum_{k=1}^{n}\sigma_i^{(k)}}{n}, \tag{30}$$

where i is the node number, n represents the number of units containing the node, and $\sigma_i^{(k)}$ is the stress of node i calculated in the k unit containing the node.

The error is defined in the form of strain energy.

$$\left\|e_\sigma\right\| = \left\|\sigma^*-\hat{\sigma}\right\| = \left(\int_{\Omega}\left(\sigma^*-\hat{\sigma}\right)^T\left(\sigma^*-\hat{\sigma}\right)d\Omega\right)^{0.5}, \tag{31}$$

where σ^* is the smooth stress vector, it is obtained by Eq. (29). $\hat{\sigma}$ is the approximate solution of the calculated stress.

According to the given target error $\left\|e_\sigma\right\|_{aim}$, calculate the new mesh cell size.

$$h = \left[\frac{\left\|e_\sigma\right\|_{aim}}{\left\|e_\sigma\right\|}\right]h_e, \tag{32}$$

where, h_e is the initial mesh cell size, and h is the modified mesh size.

The specific combination of mesh reconstruction technology and extended finite element is as follows.

As shown in Fig. 2, firstly, the structural model was established according to the finite element software, and the nodes and elements of the mesh were extracted. Secondly, the SIFs were obtained by solving the integral equation through the XFEM. Then, based on the solution results of the XFEM and the mesh data of the model, the error was compared with the target error. When the calculation error is greater than the target error, the calculation accuracy is insufficient, thus the mesh needs to be re-divided and the above process needs to be repeated. If it is less than the aim error, it indicates that the accuracy meets the next expansion demand, and the SIFs can be used for path prediction.

5. Simulation verification

In this section, two models with cracks are studied to verify the reliability of the proposed method. The first case is a square plate with a horizontal crack. The second case is a square plate with an oblique crack. We compare the calculated results with the numerical results to verify the reliability of the proposed method. At the same time, the comparison between the adaptive extended finite element method and the extended finite element method in each calculation example is compared.

Case one. Single crack stretching

In this case, a square plate with a horizontal crack is studied. The crack location of the square plate is shown in Fig. 3. The starting point of the crack is located in the center of the left boundary of the square plate, and the crack length is *a*. The upper boundary of the plate is uniformly subjected to a load of size σ. The geometric dimensions are as follows.

1) , $a/W = 0.2, 0.3, 0.4, 0.5$

2) $H/W = 0.4, 1, 2$.

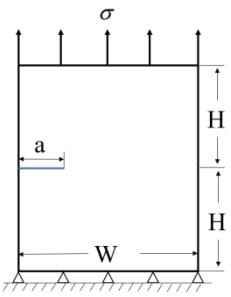

Fig. 3 Single straight crack plate

The mesh was divided by quadrilateral elements, and the mesh sizes of crack propagation paths and other positions were as follows.

The approximate global size is $h_1 = 3$.The approximate element size of the crack growth region is $h_2 = 1$.

$$K_I = F\sigma\sqrt{\pi a}\,, \tag{33}$$

$$F = 1.12 - 0.231\frac{a}{W} + 10.55\left(\frac{a}{W}\right)^2 - 21.72\left(\frac{a}{W}\right)^3 + 30.39\left(\frac{a}{W}\right)^4. \tag{34}$$

The plate width is fixed, and according to Eq. (33) and Eq. (34), H/W is unique when a/W is unchanged.

The normalized SIF are shown in Table 1

Table 1
Normalized SIF for the single crack of square tensile plate

H/W	a/W			
	0.2	0.3	0.4	0.5
0.4	1.4429	1.8064	2.1567	2.9210
1	1.2807	1.6589	2.1123	2.8457
2	1.3220	1.6207	2.0479	2.7197
Eq. (50)	1.3709	1.6602	2.1039	2.8269

As shown in Table 1, the calculated results of the proposed method are very close to analytical solutions. At the same time, it is not difficult to find that the influence of H/W is very necessary for the calculation of stress intensity factor. Under the same ratio of a/W, little H/W will lead to larger errors of SIFs, even when a/W = 0.2 and H/W = 0.4, the SIF is 8.38% larger than that when a=2. With the increase of H/W, the calculation error decreases. For example, when a/W = 0.5 and H/W = 2, the error is only 0.038%.In addition, it can be seen from Table 1 that when $H/W > 2$, the deviation between the calculated results and the analytical solution results is small, it can be considered that no matter what value *a/W* is, the influence of *H/W* on the SIF is negligible.

To ensure the accuracy of calculation, the target error of edge crack is set to 3% in the error analysis. By comparing the crack growth path, the rationality and reliability of the proposed method are confirmed. The specific constraints on model parameters, meshing, and crack growth are as follows.

i. Select the scale coefficient of square plate size as $H/W = 1$, $a/W = 0.3$. The specific parameters are as follows. Plate W = 20 mm, plate length $2H$ = 40 mm, preset crack length a = 6 mm, crack starting and ending point coordinates (0,20), (6,20). The parameters of the material are set as, Poisson's ratio $\nu = 0.3$, and Young's modulus E = 1000 MPa. Select plane strain state. Since the normalized SIF was calculated in this paper, the applied load σ could not affect the result, the unit load σ = 1 MPa is applied.

ii. The crack is set to expand by 2 mm each time. This case is compared with the initial crack and its third propagation.

The crack tip stress error of the prefabricated crack in the extended finite element method is 2.1668%, after the first step is 3.2013%, after the second step is 4.4654%, and after the third step is 5.8371%. The number of mesh nodes and units is 328 and 304.

The first mesh reconstruction is as follows. The cell size was refined with 0.3, and the number of mesh nodes and elements was 480 and 458. The crack tip stress error of the first extension was calculated as 2.1269%, and that after the second extension was calculated as 3.0758%.

The second mesh reconstruction is as follows. The cell size is refined to 0.1, and the number of mesh nodes and elements is 848 and 826. The crack tip stress error at the end of the second extension is 2.9449%. The third extension condition is satisfied.

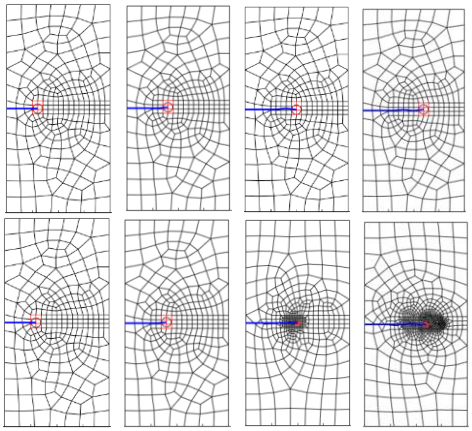

Fig. 4 Comparison of direct crack path growth

Fig. 4 shows the comparison between the extended finite element method and the adaptive extended finite element method. In the comparison figures, the extended finite element method is on the top and the adaptive extended finite element method is on the bottom. The red area in the figures is the mesh area occupied by the radius of the crack tip strengthening radius *r*. Since the mesh needs to be recalculated and expanded each time after reconstruction, there will be insignificant errors in the process of illustration. According to the calculation accuracy, sub-errors can be ignored.

Case two. Single inclined crack plate stretching

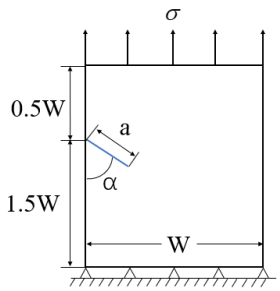

Fig. 5 Single inclined crack plate

In this case, a square plate with an oblique crack is studied. The crack location of the square plate is shown in Fig. 5. The starting point of the crack is located on the left boundary of the square plate, 1.5 times wider from the bottom edge and 1 times wider from the top. The crack length is a and the angle between the crack and the plate boundary is α .

Considering the following scenarios

1) $a/W = 0.3, 0.4, 0.5$,

2) $\alpha = 45^{o}, 67.5^{o}$.

The mesh elements were still quadrilateral, and the area of the oblique crack growth path was refined separately during the partition. The meshing strategy is the same as in Case one. An oblique crack is a compound crack propagation under tensile expansion. The normalized stress intensity factors of type *I* and *II* at 45° and 67.5° are given in Tables 2 and 3.

Comparisons of SIFs results at oblique cracks at 67.5° and 45° with the SIFs Manuals [39] and Aliabadi [40] et al described in Figs. 6 and 7. As can be seen from the data and curves, the calculated results of the proposed method are very close to those of the proposed method. For the type *I* and type *II* SIFs of the cracks, the maximum error between the proposed results and the other two results is 8% and the minimum error compared with reference SIFs Manuals [39] and Aliabadi [40] et al is 0.9% and 0.4%, respectively. It shows that the method in this paper can calculate the stress intensity factor with high precision.

Table 2

The mode I normalized SIF of oblique crack

Angle α	a/W		
	0.3	0.4	0.5
45°	0.839	0.949	1.382
67.5°	1.447	1.755	2.302

Table 3

The type II normalized SIF of oblique crack

Angle α	a/W		
	0.3	0.4	0.5
45°	0.448	0.528	0.587
67.5°	0.357	0.434	0.543

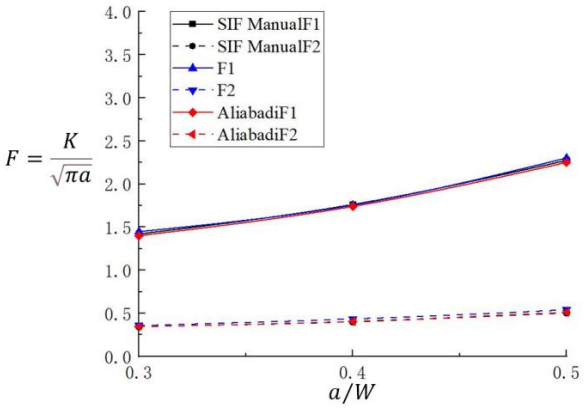

Fig. 6 Normalized SIF of mode *I*, *II* when the angle is 67.5°

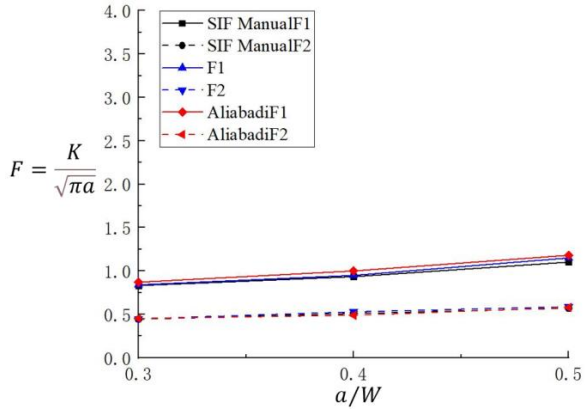

Fig. 7 Normalized SIF of mode *I*, *II* when the angle is 45°

The specific constraints on the parameters, meshing, and crack growth of the oblique crack model are as follows.

i.The specific parameters are as follows. Plate width $W = 20$ mm, plate length $2.5H = 50$ mm, present crack length $a = 6$ mm, the coordinate of crack origin (0,30), and

angle between crack and plate boundary α=45°. The material parameters are the same as those of the single crack model.

ii. The crack was set to expand by 2 mm each time. This case was compared with the initial crack and its third propagation.

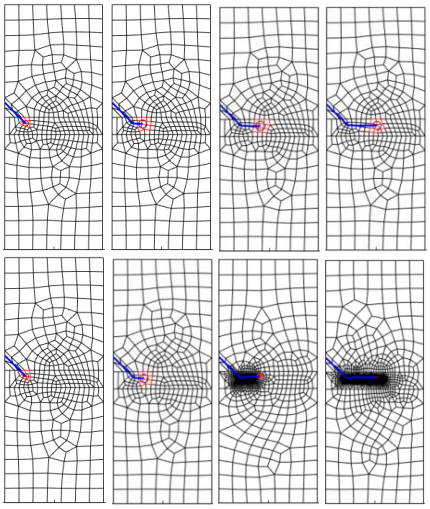

Fig. 8 Comparison of oblique crack path growth

The crack tip stress error of the prefixed crack in the XFEM is 3.8981%, 6.0322% after the first step, and 8.4715% after the second step. The number of mesh nodes and elements is 344 and 319.

The first mesh reconstruction is follows. The cell size was refined to 0.3, and the number of mesh nodes and elements was 1253 and 1228. The crack tip stress error after the first extension was recalculated as 3.831%, and that after the second extension was 5.2098%.

The second mesh reconstruction follows. The refinement strategy of the previous step was retained and the cell size was refined to 0.1, and the number of mesh nodes and elements was obtained as 2002 and 1977. The crack tip stress error at the end of the second extension was 4.709%. The third extension is now satisfied.

It can be seen that before the adaptive algorithm is combined, the error at the crack tip does not meet the calculation requirements at the end of the first step, and with the crack growth error increasing significantly, the error at the end of the third expansion is more than double of the target error. Without the combination of adaptive crack path downward slightly inclined, after mesh refinement of the crack path, this will be adjusted in the next propagation of the path to a straight line.

6. Conclusions

In this paper, a crack analysis method based on XFEM and mesh adaptive reconstruction technique is proposed. In this method, the advantages of extended finite elements in crack analysis and the improvement of the calculation accuracy of adaptive finite elements are combined to achieve a more accurate crack growth prediction. By calculating the static stress intensity factors of straight crack and oblique crack, the accuracy of the proposed method for treating different crack types is verified. By comparing the results of the extended finite element and the adaptive extended finite element, it is shown that the adaptive method can improve the calculation accuracy and verify the accuracy of the proposed method in predicting the crack growth path.

Acknowledgments

This work was partly supported by the National Natural Science Foundation of China (12302270, 52075500, and 52175256), partly by key scientific and technological project of Henan Province (232102221040, 232102221041, and 232102221033), and partly by Key Research Project Plan for Higher Education Institutions in Henan Province（23A460001).

References

1. **Shin, H.; Thamburaja, P.; Srinivasa, A.R.** 2023. Modeling impact fracture in a quasi-brittle solid using a 3D nonlocal graph-based finite element analysis: Theory, finite element simulations, and experimental verification, Journal of the Mechanics and Physics of Solids 170: 105097. https://doi.org/10.1016/J.JMPS.2022.105097.
2. **Li, Z.; Han, F.** 2023. The peridynamics-based finite element method (PeriFEM) with adaptive continuous/discrete element implementation for fracture simulation, Engineering Analysis with Boundary Elements 146: 56-65. https://doi.org/10.1016/J.ENGANABOUND.2022.09.033.
3. **Ilie, P.; Ince, A.** 2022. Three‐dimensional fatigue crack growth simulation and fatigue life assessment based on finite element analysis, Fatigue & Fracture of Engineering Materials & Structures 45(11): 3251-3266. https://doi.org/ 10.1111/FFE.13815.
4. **Ban, C.; Pu, N.; Zhang, Y.** 2022. A linear smoothed meshfree method with intrinsic enrichment functions for 2D crack analysis, Engineering Computations 39(7): 2449-2482. https://doi.org/ 10.1108/EC-02-2021-0072.
5. **Jiang, S.; Gu, Y.; Golub, M.V.** 2022. An efficient meshless method for bimaterial interface cracks in 2D thin-layered coating structures, Applied Mathematics Letters 131: 108080. https://doi.org/ 10.1016/J.AML.2022.108080.
6. **Liaghat, F.; Khosravifard, A.; Hematiyan, M.R.** 2021. A practical meshfree inverse method for identification of thermo-mechanical fracture load of a body by examining the crack path in the body, Engineering Analysis with Boundary Elements 133: 236-247. https://doi.org/10.1016/J.ENGANABOUND.2021.08.029.
7. **Xie, G.; Wang, L.; Zhang, J.;** et al. 2015. Calculation of three-dimensional nearly singular boundary element integrals for steady-state heat conduction, Engineering Analysis with Boundary Elements 60: 137-143. https://doi.org/ 10.1016/j.enganabound.2014.12.008.
8. **Gu, Y.; Hua, Q.; Chen, W.; Zhang C.** 2016. Numerical evaluation of nearly hyper-singular integrals in the boundary element analysis, Computers & Structures 167: 15-23. https://doi.org/ 10.1016/j.compstruc.2016.01.017.

9. **Zvyagin, A.V.; Udalov, A.S.; Shamina, A.A.** 2022. Boundary element method for investigating large systems of cracks using the Williams asymptotic series, Acta Astronautica 194: 480-487. https://doi.org/10.1016/J.ACTAASTRO.2021.11.024.
10. **Santos, S.A.; Daros, C.H.** 2022. Boundary element method applied to three-dimensional crack analysis in exponentially graded viscoelastic materials, Engineering Fracture Mechanics 263: 108284. https://doi.org/10.1016/J.ENGFRACMECH.2022.108284.
11. **Bordas, S.P.; Rabczuk, T.; Hung, N.X.;** et al 2010. Strain smoothing in FEM and XFEM, Computers & structures 88(23-24): 1419-1443. https://doi.org/10.1016/j.compstruc.2008.07.006.
12. **Feng, S.; Han X.; Li Z.;** et al**.** 2022. Ensemble learning for remaining fatigue life prediction of structures with stochastic parameters: A data-driven approach, Applied Mathematical Modelling 101: 420-431. https://doi.org/10.1016/J.APM.2021.08.033.
13. **Feng, S.; Han, X.; Ma, Z.;** et al**.** 2020. Data-driven algorithm for real-time fatigue life prediction of structures with stochastic parameters, Computer Methods in Applied Mechanics and Engineering 372: 113373. https://doi.org/10.1016/j.cma.2020.113373.
14. **Atluri, S.N.; Zhu, T.** 1998 A new meshless local Petrov-Galerkin (MLPG) approach in computational mechanics, Computational mechanics 22(2): 117-127. https://doi.org/10.1007/s004660050346.
15. **Gu, Y.; Chen, W.; Zhang B.** 2015. Stress analysis for two-dimensional thin structural problems using the meshless singular boundary method, Engineering Analysis with Boundary Elements 59: 1-7. https://doi.org/10.1016/j.enganabound.2015.03.017.
16. **Usman, M.; Uddin, M.; Lamichhane, A.;** et al. 2021. Meshless method of approximate particular solution for an initial and boundary value problem of the Korteweg–de Vries type equation and eventual periodicity, Partial Differential Equations in Applied Mathematics 4: 100088. https://doi.org/10.1016/J.PADIFF.2021.100088.
17. **Zhou, W.; Liu, B.; Wang, Q.;** et al. 2020. Formulations of displacement discontinuity method for crack problems based on boundary element method, Engineering Analysis with Boundary Elements 115: 86-95. https://doi.org/10.1016/j.enganabound.2020.03.007.
18. **Xie, G.; Zhou, F.; Li, H.;** et al. 2019. A family of non-conforming crack front elements of quadrilateral and triangular types for 3D crack problems using the boundary element method, Frontiers of Mechanical Engineering 14(3). 332-341. https://doi.org/10.1007/s11465-019-0540-3.
19. **Xie, G.; Zhou, F.; Zhong, Y.; Geng, H.; Wu, C.** 2020. Bi-directional sinh transformations based on the generalized Duffy space for nearly singular integrals, Journal of Computational and Applied Mathematics 380: 112981. https://doi.org/10.1016/j.cam.2020.112981.
20. **Jena, J.; Singh, S.; Gaur, V.;** et al**.** 2021. A new framework based on XFEM for cracked semipermeable piezoelectric material, Engineering Fracture Mechanics 253: 107874. https://doi.org/10.1016/J.ENGFRACMECH.2021.107874.
21. **Bybordiani, M.; Latifaghili, A.; Soares, Jr.D.;** et al. 2021. An XFEM multilayered heaviside enrichment for fracture propagation with reduced enhanced degrees of freedom, International Journal for Numerical Methods in Engineering 122(14): 3425-3447. https://doi.org/10.1002/NME.6669.
22. **Bordas, S.; Moran, B.** 2006. Enriched finite elements and level sets for damage tolerance assessment of complex structures, Engineering Fracture Mechanics 73(9): 1176-1201. https://doi.org/10.1016/j.engfracmech.2006.01.006.
23. **Moës, N.; Dolbow, J.; Belytschko, T.** 1999. A finite element method for crack growth without remeshing, International journal for numerical methods in engineering 46(1): 131-150. https://doi.org/10.1002/(SICI)1097-0207(19990910)46:1<131::AID-NME726>3.0.CO;2-J.
24. **Budyn, E.; Zi, G.; Moës, N.;** et al. 2004. A method for multiple crack growth in brittle materials without remeshing, International journal for numerical methods in engineering 61(10): 1741-1770. https://doi.org/10.1002/nme.1130.
25. **Wells, G.N.; Sluys, L.J.** 2001. A new method for modelling cohesive cracks using finite elements, International Journal for numerical methods in engineering 50(12): 2667-2682. https://doi.org/10.1002/nme.143.
26. **Zi, G.; Belytschko, T.** 2003. New crack‐tip elements for XFEM and applications to cohesive cracks, International Journal for Numerical Methods in Engineering 57(15): 2221-2240. https://doi.org/10.1002/nme.849.
27. **Asferg, J.L.; Poulsen, P.N.; Nielsen, L.O.** 2007. A consistent partly cracked XFEM element for cohesive crack growth, International Journal for Numerical Methods in Engineering 72(4): 464-485. https://doi.org/10.1002/nme.2023.
28. **Xie, G.; Jia, H.; Li, H.;** et al. 2023. A life prediction method of mechanical structures based on the phase field method and neural network, Applied Mathematical Modelling 119: 782-802. https://doi.org/10.1016/J.APM.2023.03.022.
29. **Bashiri, A.H.; Alshoaibi A, M.** 2020. Adaptive finite element prediction of fatigue life and crack path in 2D structural components, Metals 10(10): 1316. https://doi.org/10.3390/met10101316.
30. **Hitti, K.; Feghali, S.; Rafeh, F.;** et al. 2018. A novel monolithic Lagrangian approach for modelling crack propagation using anisotropic mesh adaptation, International Journal of Advances in Applied Mathematics and Mechanics 5(3): 53-65.
31. **Nicolas, G.; Fouquet, T.; Geniaut, S.;** et al. 2016. Improved adaptive mesh refinement for conformal hexahedral meshes, Advances in Engineering Software 102: 14-28. https://doi.org/10.1016/j.advengsoft.2016.07.014.
32. **Wang, Q.; Zhou, W.; Cheng, Y.;** et al. 2017. An adaptive cell-based domain integration method for treatment of domain integrals in 3D boundary element method for potential and elasticity problems, Acta Mechanica Solida Sinica 30(1): 99-111. https://doi.org/10.1016/j.camss.2016.08.002.

33. **Teng, Z.; Sun, F.; Wu, S.;** et al. 2018. An adaptively refined XFEM with virtual node polygonal elements for dynamic crack problems, Computational Mechanics 62(5): 1087-1106. https://doi.org/10.1007/s00466-018-1553-1.
34. **Shao, Y.; Duan, Q.; Qiu, S.** 2020. Consistent element-free Galerkin method for three-dimensional crack propagation based on a phase-field model, Computational Materials Science 179: 109694. https://doi.org/10.1016/j.commatsci.2020.109694.
35. **De Oliveira Miranda, A.C.; Meggiolaro, M.A.; Martha, L.F.; De Castro, J.T.P.** 2012. Stress intensity factor predictions: Comparison and round-off error, Computational materials science 53(1): 354-358. https://doi.org/10.1016/j.commatsci.2011.09.033.
36. **Wang, Z.; Yu, T.; Bui, T.;** et al. 2016. Numerical modeling of 3-D inclusions and voids by a novel adaptive XFEM, Advances in Engineering Software 102: 105-122. https://doi.org/10.1016/j.advengsoft.2016.09.007.
37. **Tabarraei, A.; Sukumar, N.** 2008. Extended finite element method on polygonal and quadtree meshes, Computer Methods in Applied Mechanics and Engineering 197(5): 425-438. https://doi.org/10.1016/j.cma.2007.08.013.
38. **Zhao, X.** 2021. A three-dimensional robust volume-of-fluid solver based on the adaptive mesh refinement, Theoretical and Applied Mechanics Letters 11(6): 100309. https://doi.org/10.1016/J.TAML.2021.100309.
39. **Murakami, Y.; Keer, L.M.** 1993. Stress intensity factors handbook, vol. 3. https://doi.org/10.1115/1.2900983.
40. **Aliabadi, M.H.; Rooke, D.P.; Cartwright D J.** 1987. Mixed-mode Bueckner weight functions using boundary element analysis, International Journal of Fracture 34(2): 131-147. https://doi.org/10.1007/BF00019768.

G. Xie, C. Zhao, H. Li, J. Liu Y. Zhong, W. Du, J. Lv, C. Wu

AN ADAPTIVE EXTENDED FINITE ELEMENT BASED CRACK PROPAGATION ANALYSIS METHOD

S u m m a r y

In this paper, a method of crack propagation analysis based on adaptive extension finite element is proposed. This method combines adaptive mesh reconstruction technology with the extended finite element method (XFEM). Firstly, the model of the engineering structure is discretized with the help of mesh generation software, and the initial mesh is divided. Secondly, the Construction of the XFEM model and the tip of the crack strengthening function are introduced to describe the physical field properties of the crack tip. The integral equation is solved to obtain the crack tip parameters. Then, the adaptive mesh reconstruction technology is built to refine the mesh of the crack tip area through the error estimation of the crack tip. Finally, the SIFs at the crack tip were calculated using the interaction integral, and the path direction of crack growth was determined using the maximum circumferential tensile stress criterion. Thus, the propagation path can be well traced.

Keywords: adaptive mesh reconstruction, crack propagation, extended finite element method, stress intensity factors.

Received January 28, 2023
Accepted February 15, 2024

This article is an Open Access article distributed under the terms and conditions of the Creative Commons Attribution 4.0 (CC BY 4.0) License (http://creativecommons.org/licenses/by/4.0/).